SOILS AND FOUNDATIONS Vol. 49, No. 2, 207–220, Apr. 2009
Japanese Geotechnical Society

NUMERICAL ANALYSIS OF FOOTING SETTLEMENT PROBLEM BY SUBLOADING SURFACE MODEL

TATSUYA MASE[i] and KOICHI HASHIGUCHI[ii]

ABSTRACT

This article addresses the numerical analysis of the load-settlement relation of footing on a soil ground by the finite difference method incorporating the subloading surface model. The subloading surface model is the elastoplastic constitutive model describing most pertinently the plastic strain rate due to the rate of stress inside the yield surface so as to fulfill the continuity and the smoothness conditions. For the finite difference program *FLAC3D* is used, which adopts the explicit dynamic relaxation method without solving the total stiffness matrix equation and thus has the capability for the remarkable reduction of calculation time. The relevance of the present approach to the description of the load-settlement curve exhibiting the ultimate load is demonstrated by the numerical experiments. Further, the applicability to the prediction of real behavior of footing-settlement is verified by comparison with the test data for sand grounds with a high friction property.

Key words: bearing capacity, constitutive equation, elastoplasticity, (footing-settlement), numerical analysis, (subloading surface model) (**IGC**: E2/E3/E13)

INTRODUCTION

The most fundamental issue in soil mechanics is the prediction of bearing capacity of soil ground. In this context, the slip-line method has been used most widely for a long time in the history of soil mechanics. However, it has the serious limitations due to the premise of the rigid-perfectly plasticity, i.e., the disregard of the elastic deformation and the hardening/softening behavior. Therefore, it predicts merely the ultimate load but is incapable of predicting a deformation at all. On the other hand, a big research effort has been made so far to develop the elastoplastic constitutive equation of soils and the numerical method for the analyses of boundary-value problems on the deformation behavior of soil structures, especially the footing-settlement problem (cf. de Borst and Vermeer, 1984; Pietruszczak and Niu, 1993; de Borst and Groen, 1999; Borja et al., 1990, 1991, 1998, 2001, 2004; Siddiquee et al., 2001; Potts, 2003; Smith and Griffith, 2004). Notwithstanding, it has not been advanced to the level to take the place of the slip-line method for the mechanical design of soil structures in practice so far. On this background there exists the difficulty in the large deformation analysis of soil structures observed typically by the settlement of footing on the soil ground with a high friction property. The difficulty would be caused by the following facts:

1) Soils are frictional materials exhibiting the pressure dependence and the plastic-volumetric change giving rise to the volumetric (dilatancy) locking behavior in the finite element analysis (cf. de Borst et al., 1993; de Borst and Groen, 1999),
2) Soils in the neighborhood of ground surface are in the heavily over-consolidated state and thus yield considerable softening behavior as the footing-settlement proceeds,
3) Soils undergo a large deformation leading to localization, i.e., shear banding when the load approaches the ultimate value.

In order to overcome these problems, the elaborated constitutive relation and numerical method would have to be adopted. The *subloading surface model* (Hashiguchi and Ueno, 1977; Hashiguchi, 1978, 1980, 1989) falling within the framework of unconventional plasticity (Drucker, 1988) has been proposed and developed to describe pertinently the plastic strain rate induced by the rate of stress inside the yield surface, fulfilling the continuity and the smoothness conditions (Hashiguchi, 1993a, b, 1997, 2000). In addition, it possesses the considerable advantages in numerical analyses: it is not required to incorporate the algorithm for judgment whether or not a stress reaches the yield surface and is equipped intrinsically with the controlling function so as to attract the stress to the yield surface so that it is not required to incorporate a return-mapping algorithm in the yield state. It has been extended so as to describe the deformation of soils in the negative range of pressure (Hashiguchi and Mase, 2007), while the past constitutive

[i] Engineer, Tokyo Electric Power Services Co, Ltd., Japan (tmase@tepsco.co.jp).
[ii] Professor, Dept. Social. Environ. Eng., Daiichi Tech. Univ., Japan.
The manuscript for this paper was received for review on April 25, 2008; approved on January 29, 2009.
Written discussions on this paper should be submitted before November 1, 2009 to the Japanese Geotechnical Society, 4-38-2, Sengoku, Bunkyo-ku, Tokyo 112-0011, Japan. Upon request the closing date may be extended one month.

equation of soils based on the subloading surface model was limited to the positive range of pressure and has involved the singular point of plastic modulus in the null stress state in which the yield and the subloading surfaces having different sizes contact with each other. Here, the Jaumann rate is incorporated as a corotational rate for sake of simplicity and thus the objectivity of constitutive equation is furnished so as not to be influenced by the rigid body rotation for the shear strain up to one hundred and several ten percents in anisotropic plastic constitutive equations involving the second-order tensor describing the kinematic or rotational hardening, while the strain is less than 10% even in the post-peak behavior of the present problem of footing settlement as will be shown in the later section.

For the finite element analysis, suitable selections of elements and integration method are required, where the popular rectangular element with 2×2 integration points causes often the shear-locking problem (cf. the comprehensive overview of de Borst et al. (1993)). The following various improvements have been proposed, while the explanation is given here for the plane strain condition.

1. The triangle elements with fifteen integration points is adopted by Sloan and Randolph (1982) and de Borst et al. (1984, 1999) in which only the over-consolidated soil ground is studied adopting the Coulomb or Drucker-Prager yield condition.
2. The rectangular elements with the reduced integration (one) point incorporating an hourglass prevention algorithm is adopted by some researchers, e.g., Smith and Griffith (2004) and Potts (2003), while their analyses are also limited to the over-consolidated soil ground without the plastic volumetric contraction.
3. The consistent return mapping method (Simo and Hughes, 1998) is adopted by Borja et al. (1990, 1991, 1998, 2001, 2004), Simo and Meschke (1993) and Yamakawa (2003). It is formulated so as to describe the finite deformation based on the multiplicative decomposition (Lee, 1969), the Hencky strain and the hyper-elastic constitutive equation. It has a quite high efficiency and accuracy in calculation. However, it is limited to the isotropy at present and the enhancement towards the description of anisotropic deformation behavior is one of the difficult problems remained in the finite strain theory for the general elastoplastic materials.
4. The rectangular elements with reduced (one point) integration and the hour-glass prevention algorithm incorporating the explicit dynamic-relaxation method is adopted by Tanaka (Tanaka and Kawamoto, 1988; Siddiquee et al., 1999, 2001). The time required for calculation can be reduced drastically since the solution of total stiffness matrix equation between the forces and the displacements of whole nodal points is not required.

The ultimate load was calculated by Noda et al. (2007) in the numerical experiment incorporating the super/subloading surface model in which the superloading surface is introduced in addition to the subloading surface in order to describe the effect of structures in soils. The relevance of the structure in soils to the appearance of ultimate load in the footing settlement behavior would require further study.

In this article the settlement behavior of footing on a soil ground is analyzed by incorporating the subloading surface model into the finite difference code *FLAC3D* (Cundall and Board, 1988; Itasca Consulting Group, 2006) which adopts the explicit dynamic-relaxation method without solving the total stiffness matrix equation and thus has the capability for the remarkable reduction of calculation time. Then, it is verified by comparison with test data for the rigid footings on sand grounds with a high friction property, that the present approach is capable of describing the footing settlement behavior rigorously and realistically up to the ultimate load.

The signs of a stress (rate) and a strain rate (a symmetric part of velocity gradient) components are taken to be positive for tension, and the stress for soils means the effective stress, i.e., the stress excluded a pore pressure from a total stress throughout this article.

OUTLINE OF SUBLOADING SURFACE MODEL

The subloading surface model (Hashiguchi and Ueno, 1977; Hashiguchi, 1978, 1980, 1989) is reviewed briefly in this section.

Denoting the current configuration of the material particle as $\mathbf{x}$ and the current velocity as $\mathbf{v}$, the velocity gradient is described as $\mathbf{L}=\partial \mathbf{v}/\partial \mathbf{x}$. The strain rate and the continuum spin are defined as $\mathbf{D}\equiv(\mathbf{L}+\mathbf{L}^{\mathrm{T}})/2$ and $\mathbf{W}\equiv(\mathbf{L}-\mathbf{L}^{\mathrm{T}})/2$, respectively, $(\ )^{\mathrm{T}}$ standing for the transpose. Limiting to the infinitesimal strain, let the strain rate $\mathbf{D}$ be additively decomposed into the elastic strain rate $\mathbf{D}^{\mathrm{e}}$ and the plastic strain rate $\mathbf{D}^{\mathrm{p}}$ as follows:

$$\mathbf{D}=\mathbf{D}^{\mathrm{e}}+\mathbf{D}^{\mathrm{p}}. \tag{1}$$

First, let $\mathbf{D}^{\mathrm{e}}$ be given simply by the hypoelastic equation, i.e.,

$$\mathbf{D}^{\mathrm{e}}=\mathbf{E}^{-1}\overset{\circ}{\boldsymbol{\sigma}}, \tag{2}$$

where $\mathbf{E}$ is the fourth-order elastic modulus tensor, $(\ )^{-1}$ denoting the inverse operation, and $\boldsymbol{\sigma}$ is the Cauchy stress. $(\overset{\circ}{})$ stipulates the proper (objective) corotational rate, while let it be given by the following Jaumann rate (Jaumann, 1911) for sake of simplicity.

$$\overset{\circ}{\boldsymbol{\sigma}}=\overset{\bullet}{\boldsymbol{\sigma}}-\mathbf{W}\boldsymbol{\sigma}+\boldsymbol{\sigma}\mathbf{W}, \tag{3}$$

where $(\overset{\bullet}{})$ stands for the material-time derivative. It should be noted that the strain rate has to be decomposed to the elastic and the plastic parts by the multiplicative decomposition (cf. Hashiguchi, 2008) and the elastic part has to be formulated as the hyper-elastic constitutive equation in the description of finite deformation. Therefore, the present theory is limited to the infinitesimal strain, while it holds for the finite rotation.

Let the following isotropic yield condition be assumed for sake of simplicity.

$$f(\boldsymbol{\sigma}) = F(H), \tag{4}$$

where F is the hardening function of isotropic hardening/softening variable H. Here, for sake of simplicity in formulation let it be assumed that $f(\boldsymbol{\sigma})$ is the homogeneous function of $\boldsymbol{\sigma}$ in degree-one. Further, the subloading surface is described by

$$f(\boldsymbol{\sigma}) = RF(H). \tag{5}$$

The material-time derivative of Eq. (5) leads to

$$\mathrm{tr}\left(\frac{\partial f(\boldsymbol{\sigma})}{\partial \boldsymbol{\sigma}} \mathring{\boldsymbol{\sigma}}\right) = \dot{R}F + RF'\dot{H}, \tag{6}$$

where

$$F' \equiv dF/dH. \tag{7}$$

Hereinafter, let $\dot{H}$ be given by

$$\dot{H} = h(\boldsymbol{\sigma}, H, \mathbf{D}^{\mathrm{p}}), \tag{8}$$

while h is the homogeneous function of $\mathbf{D}^{\mathrm{p}}$ in degree-one since the time-independent deformation is concerned. The direct transformation of the material-time derivative to the corotational derivative used in Eq. (6) is verified for the general scalar-valued tensor function (Hashiguchi, 2007).

The following evolution equation of the normal-yield ratio R is given by

$$\dot{R} = U(R)\|\mathbf{D}^{\mathrm{p}}\| \quad \text{for } \mathbf{D}^{\mathrm{p}} \neq \mathbf{0}, \tag{9}$$

where U is a monotonically decreasing function of R, fulfilling the following conditions

$$U(R) = \begin{cases} \infty & \text{for } R = 0, \\ >0 & \text{for } 0 < R < 1, \\ 0 & \text{for } R = 1, \\ (>0 & \text{for } R > 1). \end{cases} \tag{10}$$

Let the function U satisfying Eq. (10) be simply given by

$$U = -u \ln R, \tag{11}$$

where u is a material constant. By virtue of incorporation of Eq. (9), a stress is automatically drawn back to the normal-yield surface even if it goes out from that surface since it is formulated that $\dot{R} > 0$ for $R < 1$ (subyield state) and $\dot{R} < 0$ for $R > 1$ (over normal-yield state) in Eq. (11) with the condition (*see* Fig. 1). Thus, a stable calculation is executed even by rough loading steps compared with the conventional models when the Euler method is adopted in numerical calculations as will be shown explicitly in the following section.

Substitution of Eq. (9) into Eq. (6) leads to the *consistency condition* for the subloading surface:

$$\mathrm{tr}\left(\frac{\partial f(\boldsymbol{\sigma})}{\partial \boldsymbol{\sigma}} \mathring{\boldsymbol{\sigma}}\right) = U\|\mathbf{D}^{\mathrm{p}}\|F + RF'\dot{H}. \tag{12}$$

Here, adopt the associated flow rule

$$\mathbf{D}^{\mathrm{p}} = \lambda \mathbf{N}, \tag{13}$$

where λ is a positive proportionality factor, and $\mathbf{N}$ is the normalized outward-normal of the subloading surface at the current stress point, i.e.,

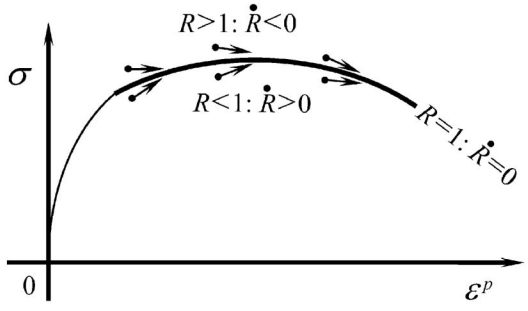

$$\dot{R} = U(R)\|\mathbf{D}^{p}\| \quad \text{for } \mathbf{D}^{p} \neq \mathbf{0}$$

$$U(R) = \begin{cases} \infty & \text{for } R = 0, \\ >0 & \text{for } 0 < R < 1, \\ 0 & \text{for } R = 1, \\ (<0 & \text{for } R > 1). \end{cases}$$

Fig. 1. Stress-controlling function equipped in the subloading surface model: The stress is automatically attracted to the normal-yield surface in the plastic loading process $\mathbf{D}^{\mathrm{p}} \neq \mathbf{0}$

$$\mathbf{N} = \frac{\partial f(\boldsymbol{\sigma})}{\partial \boldsymbol{\sigma}} \Big/ \left\| \frac{\partial f(\boldsymbol{\sigma})}{\partial \boldsymbol{\sigma}} \right\|. \tag{14}$$

The substitution of Eq. (13) into the consistency condition (12) leads to

$$\lambda = \frac{\mathrm{tr}\,(\mathbf{N}\mathring{\boldsymbol{\sigma}})}{M^{\mathrm{p}}}, \tag{15}$$

and thus the plastic strain rate is given by

$$\mathbf{D}^{\mathrm{p}} = \frac{\mathrm{tr}\,(\mathbf{N}\mathring{\boldsymbol{\sigma}})}{M^{\mathrm{p}}}\mathbf{N}, \quad \mathbf{N} \equiv \frac{\partial f(\boldsymbol{\sigma})}{\partial \boldsymbol{\sigma}} \Big/ \left\| \frac{\partial f(\boldsymbol{\sigma})}{\partial \boldsymbol{\sigma}} \right\| \tag{16}$$

where the plastic modulus M^{p} is given by

$$M^{\mathrm{p}} \equiv \left(\frac{F'}{F}h + \frac{U}{R}\right)\mathrm{tr}\,(\mathbf{N}\boldsymbol{\sigma}), \tag{17}$$

and h is the homogeneous function of $\mathbf{N}$ in degree-one which is related to $\dot{H}$ as

$$\dot{H} = \lambda h(\boldsymbol{\sigma}, H, \mathbf{N}). \tag{18}$$

The strain rate is given from Eqs. (1), (2) and (16) as follows:

$$\mathbf{D} = \mathbf{E}^{-1}\mathring{\boldsymbol{\sigma}} + \frac{\mathrm{tr}\,(\mathbf{N}\mathring{\boldsymbol{\sigma}})}{M^{\mathrm{p}}}\mathbf{N} \tag{19}$$

from which the positive proportionality factor in terms of strain rate, rewriting by Λ, is described as

$$\Lambda = \frac{\mathrm{tr}\,(\mathbf{NED})}{M^{\mathrm{p}} + \mathrm{tr}\,(\mathbf{NEN})}. \tag{20}$$

The stress rate is given from Eqs. (15), (19) and (20) as

$$\mathring{\boldsymbol{\sigma}} = \mathbf{ED} - \mathbf{E}\frac{\mathrm{tr}\,(\mathbf{NED})}{M^{\mathrm{p}} + \mathrm{tr}\,(\mathbf{NEN})}\mathbf{N}. \tag{21}$$

The loading criterion is given as follows (Hill, 1967;

Hashiguchi, 2000):

$$\left.\begin{aligned}&\mathbf{D}^{\mathrm{P}}\neq\mathbf{0}\text{: }\Lambda>0,\\&\mathbf{D}^{\mathrm{P}}=\mathbf{0}\text{: }\Lambda\leq 0.\end{aligned}\right\}\tag{22}$$

The bounding surface model with the radial-mapping (Dafalias and Herrmann, 1982) has a similar structure as the subloading surface model (Hashiguchi and Ueno, 1977) outlined in this section. However, it is impertinently formulated without any consistency condition because it does not incorporate the subloading surface. Then, it is not guaranteed for the stress to be attracted to the yield surface in the plastic deformation process. Furthermore, it cannot be adopted to describe the cyclic loading behavior, predicting the open hysteresis loop leading to the excessive strain accumulation, while the subloading surface model has been extended to describe pertinently the cyclic loading behavior as the extended subloading surface model (Hashiguchi, 1989).

MATERIAL FUNCTIONS FOR SOILS

The subloading surface is indeterminate at the null stress state for the past normal-yield surface passing through the zero stress at which the normal-yield and the subloading surfaces contact with each other at one point, resulting in the singularity of plastic modulus. In order to avoid this defect the following normal-yield surface is proposed by Hashiguchi and Mase (2007), which exhibits the ellipsoid translated to the direction of negative pressure by $-\xi F$ (ξ: material constant) as shown in Fig. 2.

$$f(p,\chi)=F,\ f(p,\chi)=\begin{cases}p\{1+(\chi/p)^2\} & \text{for } \xi=0,\\ \dfrac{1}{\bar{\xi}}(p_\chi-\bar{\xi}p) & \text{for } \xi=0,\end{cases}\tag{23}$$

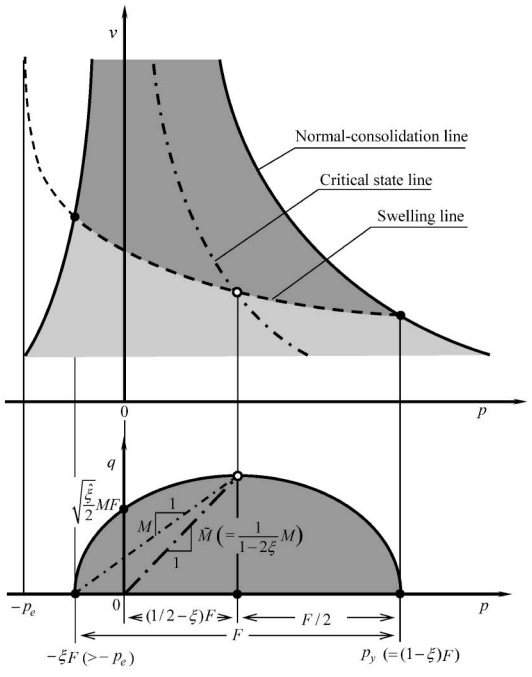

Fig. 2. Normal-yield surface of soils in the (p, q) plane

where

$$\hat{\xi}\equiv 2(1-\xi)\xi,\ \bar{\xi}\equiv(1-2\xi),\ p_\chi\equiv\sqrt{p^2+2\hat{\xi}\chi^2},\tag{24}$$

$$p\equiv-\frac{1}{3}\operatorname{tr}\boldsymbol{\sigma},\ \boldsymbol{\sigma}'\equiv\boldsymbol{\sigma}-\frac{1}{3}(\operatorname{tr}\boldsymbol{\sigma})\mathbf{I},\tag{25}$$

$$\chi\equiv\frac{\|\boldsymbol{\eta}\|}{M},\ \boldsymbol{\eta}\equiv\frac{\boldsymbol{\sigma}'}{p},\tag{26}$$

$\mathbf{I}$ is the identity tensor having the components of Kronecker's delta δ_{ij}, i.e., $\delta_{ij}=1$ for $i=j$ and $\delta_{ij}=0$ for $i\neq j$. M is the stress ratio $\|\boldsymbol{\eta}\|$ in the critical state, which is generally a function f_m of

$$\cos 3\theta_\sigma\equiv\sqrt{6}\operatorname{tr}\mathbf{t}'^3,\ \mathbf{t}'\equiv\frac{\boldsymbol{\sigma}'}{\|\boldsymbol{\sigma}'\|},\tag{27}$$

including the material constant ϕ_c referred to as the frictional angle in the critical state for the axisymmetric compression and it is given by Hashiguchi (2002) as follows:

$$M=\frac{14\sqrt{6}\sin\phi_c}{(3-\sin\phi_c)(8+\cos 3\theta_\sigma)}.\tag{28}$$

In the above, the yield surface of soils is formulated so as to fulfill the conditions 1)–3) based on the modified Cam-clay model (Roscoe and Burland, 1968). It is difficult to derive the other yield surface fulfilling the conditions 1)–3). For instance, consider the translation of the original Cam-clay model (Schofield and Wroth, 1968) to the negative pressure range by $p\to p+\xi F$.

$$(p+\xi F)\exp\left(\frac{\|\boldsymbol{\sigma}'\|}{p+\xi F}\Big/M\right)=F\tag{29}$$

However, a separated form of the stress and internal variables and the hardening function cannot be derived from this equation. On the other hand, the translation of the yield surface to the negative pressure range by the constant value C_y($p\to p+C_y$) is adopted for constitutive equations for unsaturated soils (e.g., Alonso et al., 1990; Simo and Meschke, 1993; Borja, 2004). The modified Cam-clay model, for instance, is described by this translation as follows:

$$\left\{\frac{p-(1/2)F+C_y}{F/2}\right\}^2+\frac{\|\boldsymbol{\sigma}'\|^2}{(MF/2)^2}=1\tag{30}$$

In this equation, the yield surface expands/contracts from/to the fixed point $\boldsymbol{\sigma}=C_y\mathbf{I}$ ($p=C_y$) on the hydrostatic axis and thus it does not fulfill the condition 2). The incorporation of this yield condition into the subloading surface model leads to the physical impertinence that the unloading is induced against the fact a large plastic deformation is induced when the stress translates towards the negative pressure direction.

Let the isotropic hardening/softening function F be given by the following equation, modifying the past formulation (Hashiguchi, 1974, 1995; Hashiguchi and Chen, 1998) so as to avoid the singularity induced at $p=0$.

$$F(H)=\left(F_0+\frac{p_e}{1-\xi}\right)\exp\frac{H}{\rho-\gamma}-\frac{p_e}{1-\xi},$$

$$\dot{H} = -\operatorname{tr}\mathbf{D}^{\mathrm{p}} - \mu' \|\mathbf{D}^{\mathrm{p}'}\| \frac{\|\boldsymbol{\sigma}'\| - M_{\mathrm{d}}|p|}{F}, \tag{31}$$

where F_0 is the initial value of F. ρ and γ (*see* Fig. 3) are the material constants describing the slopes of the normal-consolidation and swelling lines, respectively, of the $\ln v - \ln(p + p_{\mathrm{e}})$ linear relation (v: volume) in the isotropic consolidation (Hashiguchi, 1974, 1995, 2008). p_{e} is the material constant, while the volume becomes infinite for $p = -p_{\mathrm{e}}$. μ' is the material constant. M_{d} is the function of $\cos 3\theta_\sigma$ and is given here in the identical form as M by

$$M_{\mathrm{d}} = \frac{14\sqrt{6}\,\sin\phi_{\mathrm{d}}}{(3-\sin\phi_{\mathrm{d}})(8+\cos 3\theta_\sigma)}, \tag{32}$$

where ϕ_{d} is the material constant. The hardening and the softening are induced for $\|\boldsymbol{\sigma}'\| > M_{\mathrm{d}}|p|$ and $\|\boldsymbol{\sigma}'\| < M_{\mathrm{d}}|p|$, respectively.

The elastic modulus $\mathbf{E}$ in Eq. (2) is given in the Hooke's type as follows:

$$\left.\begin{aligned} E_{\mathrm{ijkl}} &= \left(K - \frac{2}{3}G\right)\delta_{\mathrm{ij}}\delta_{\mathrm{kl}} + G(\delta_{\mathrm{ik}}\delta_{\mathrm{jl}} + \delta_{\mathrm{il}}\delta_{\mathrm{jk}}), \\ (\mathbf{E}^{-1})_{\mathrm{ijkl}} &= \frac{1}{3}\left(\frac{1}{3K} - \frac{1}{2G}\right)\delta_{\mathrm{ij}}\delta_{\mathrm{kl}} + \frac{1}{4G}(\delta_{\mathrm{ik}}\delta_{\mathrm{jl}} + \delta_{\mathrm{il}}\delta_{\mathrm{jk}}), \end{aligned}\right\} \tag{33}$$

where the elastic bulk modulus K and the elastic shear modulus G are given as

$$K = \frac{p + p_{\mathrm{e}}}{\gamma}, \quad G = \frac{3(1-2\nu)}{2(1+\nu)}K, \tag{34}$$

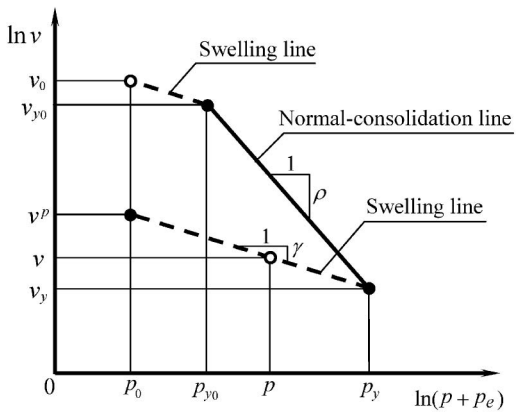

Fig. 3. ln v-ln p linear relation of isotropic consolidation of soils

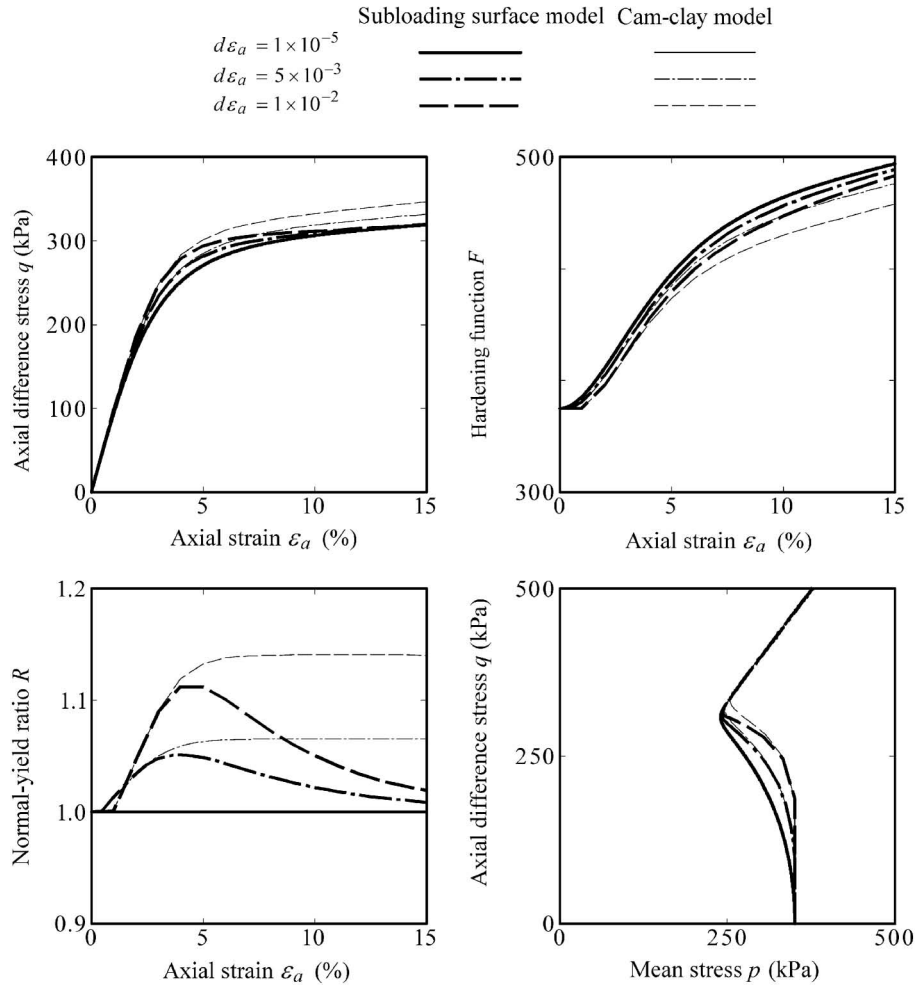

Fig. 4. Numerical results calculated by Euler method at several levels of strain increment for the triaxial compression of normally-consolidated soil by Cam-clay model and the subloading surface model

where ν is Poisson's ratio. The elastic bulk modulus in Eq. $(34)_1$ as well as Eq. (31) is derived from the $\ln \nu - \ln (p + p_e)$ linear relation of the isotropic consolidation.

The numerical results of the axial difference stress $q(= \sigma_l - \sigma_a$; σ_a: axial stress, σ_l: lateral stress), the isotropic hardening function F and the normal-yield ratio R vs. the axial strain ε_a and the stress path in the (p, q) plane for the three levels of strain increment in the undrained triaxial compression of the normally-consolidated soil are shown in Fig. 4, while the Euler method without a convergence algorithm is adopted. The following material parameters are used in the calculation.

$$F_0 = 350 \text{ kPa}, \ \phi_c = 32°, \ \xi = 0.001,$$
$$\rho = 0.1, \ \gamma = 0.05,$$
$$p_e = 0.01 \text{ kPa}, \ \nu = 0.3,$$
$$\phi_d = 29°, \ \mu' = 0.8,$$
$$u = 15.0.$$

The axial stress difference and the normal-yield ratio are predicted to go over the accurate values but inversely the hardening function is predicted to be suppressed from the accurate value as the axial strain increment increases as shown in this figure.

The stress is attracted to the normal-yield surface even if the stress goes over it by the large strain increments in the subloading surface model. Then, an accurate calculation can be performed by the subloading surface model by virtue of the controlling function.

NUMERICAL ANALYSIS OF FOOTING-SETTLEMENT BEHAVIOR

Numerical analysis of the present problem, i.e., the prediction of peak load and post-peak behavior for the footing-settlement problem on sands having the high friction and dilatancy cannot be attained in fact by the usual implicit finite element method requiring the repeated calculations of total stiffness equation which needs quite large calculation time. On the other hand, it can be attained by the explicit dynamic relaxation method in which the dynamic equilibrium equation is solved directly without solving the total stiffness equation so that the calculation time is drastically reduced. The FLAC3D (Fast Lagrangian Analysis of Continua in 3 Dimensions) (Cundall and Board, 1988; Itasca Consulting Group, 2006) based on the explicit dynamic relaxation method is adopted in the present analysis, in which the subloading surface model with the automatic controlling function to attract the stress to the normal-yield surface is implemented as the constitutive equation. The calculation is executed by the Euler method without a calculation for convergence in this program by adopting small incremental steps so as not to have an influence on the calculation, while this fact is examined prior to the calculation. The finite elements are composed of eight-noded cuboidal elements. Each cuboidal element is divided into the two kinds of overlays, i.e., assembly of five tetrahedral sub-elements having different directions as shown in Fig. 5. Then, the deviatoric variables are analyzed using individual values in each tetrahedral sub-element. On the other hand, isotropic variables are analyzed using averaging values in ten tetrahedral sub-elements in order to avoid the over-constraint problems common in finite element calculations for dilatant materials, i.e., the *dilatancy locking*.

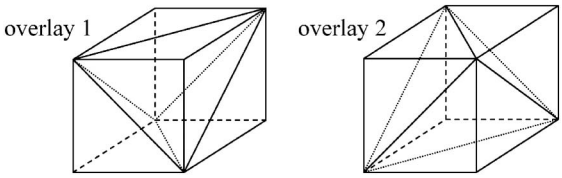

Fig. 5. An eight-noded cuboidal element with two kinds of overlays consisting of five tetrahedra

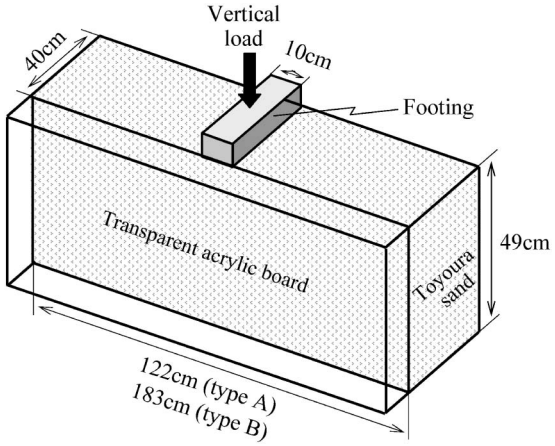

Fig. 6. Footing settlement test apparatus: type A (Tatsuoka et al., 1984) and type B (Tani, 1986)

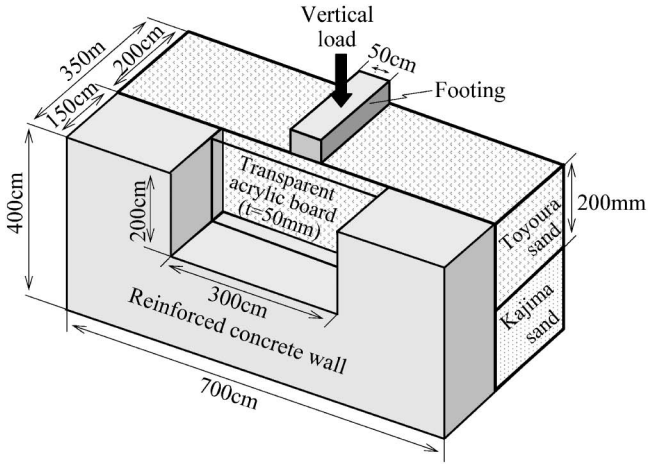

Fig. 7. Footing settlement test apparatus: type C (Okahara et al., 1989)

Test Data Used for Numerical Simulation

The test data of footing settlement phenomenon on sand layers under the plane strain condition are used for the simulation by the FLAC3D incorporating the subloading surface model explained in the preceding section.

The overviews of the test apparatus of type A (Tatsuoka et al., 1984) and type B (Tani, 1986) are shown in Fig. 6, and that of type C (Okahara et al., 1989) is shown in Fig. 7. For the large test apparatus: type C, the reinforced concrete is used for the front transparent wall in order to maintain steadily the plane strain condition and thus more accurate test data could be obtained. The footings width, denoted as B, is taken 10 cm for the types A and B and 50 cm for the type C. The sand layers have been prepared carefully by the air-pluviation method for the dried Toyoura sand in order to obtain the same homogeneous layers but the test data exhibit dispersion more or less test by test despite the laborious preparation work.

Numerical Analysis and Comparison with Test Data

The finite element meshes in the present analyses for the simulations of the test data are shown in Fig. 8. The nodal points of soil layer in contact with the footing and the bottom of soil bin are fixed to them, respectively. On the other hand, the nodal points at the side walls can move freely in the vertical direction. The right half of soil layer is analyzed in order to reduce the calculation time as has been done widely even for searching the localized deformation (cf. e.g., Sloan and Randolph, 1982; Pietruszczak and Niu, 1993; Stallebrass et al., 1997; Borja and Tamagnini, 1998; Siddiquee et al., 1999; de Borst and Groen, 1999; Sheng et al., 2000; Borja et al., 2001, 2003; Nakano et al., 2008). The symmetry of deformation would hold approximately as observed also in experiments (Tatsuoka et al., 1984; Tani, 1986; Okahara et al., 1989) used here for comparisons with predictions, while it should be noted that an analysis of only a half part is not allowed in such a problem as a buckling phenomenon searching a deformation to a lateral direction. First, the initial state of stress is chosen to be zero and then the gravity force is gradually applied to the nodal points prior to the settlement of footing. Then, the vertical displacement of footing is given by incremental steps of $10^{-5} \sim 5 \times 10^{-4}$ cm.

The material parameters in the subloading surface model are selected as:

$$F_0 = 350 \text{ kPa}, \ \phi_c = 30°, \ \xi = 0.001,$$
$$\rho = 0.0015, \ \gamma = 0.00015,$$
$$p_e = 0.01 \text{ kPa}, \ \nu = 0.3,$$
$$\phi_d = 29°, \ \mu' = 0.2,$$
$$u = 15.0.$$

referring to the values listed in the previous paper (Setouchi and Hashiguchi, 2006). The material constants ρ and γ are determined so as to fit to the inclinations of normal-consolidation line and the swelling line, respectively, in the isotropic consolidation lines depicted in the both logarithmic diagram of pressure and volume. The initial value F_0 is determined as the pressure in the transitional point from the swelling line to the normal-consolidation line in the diagram. The oedometer test data may be referred for the determination of these parameters when isotropic consolidation test datum is not at hand.

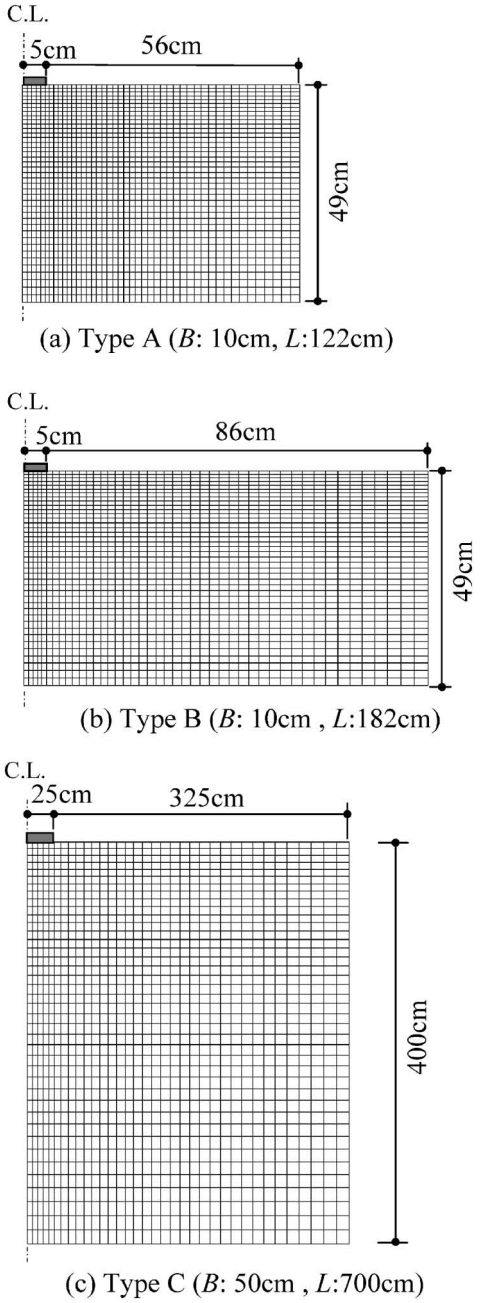

Fig. 8. Finite element meshes

The Poisson's ratio ν is determined such that the axial stress-strain equation fits the inclination of the initial rising part of stress-strain curve in the test data of the triaxial compression with a constant lateral stress, whilst the value of γ determined beforehand is used. The material constant u in the evolution rule of the normal-yield ratio R is determined so as to fit to the curvature of the stress-strain curve in the transitional state from the elastic to the normal-yield state, while it is smaller for looser materials. The material constant ϕ_c describing the angle of internal friction in the critical state as the non-cohesive material can be determined from the stress ratio in the residual state in the triaxial compression test data. The material constant ϕ_d is determined so as to describe the undrained

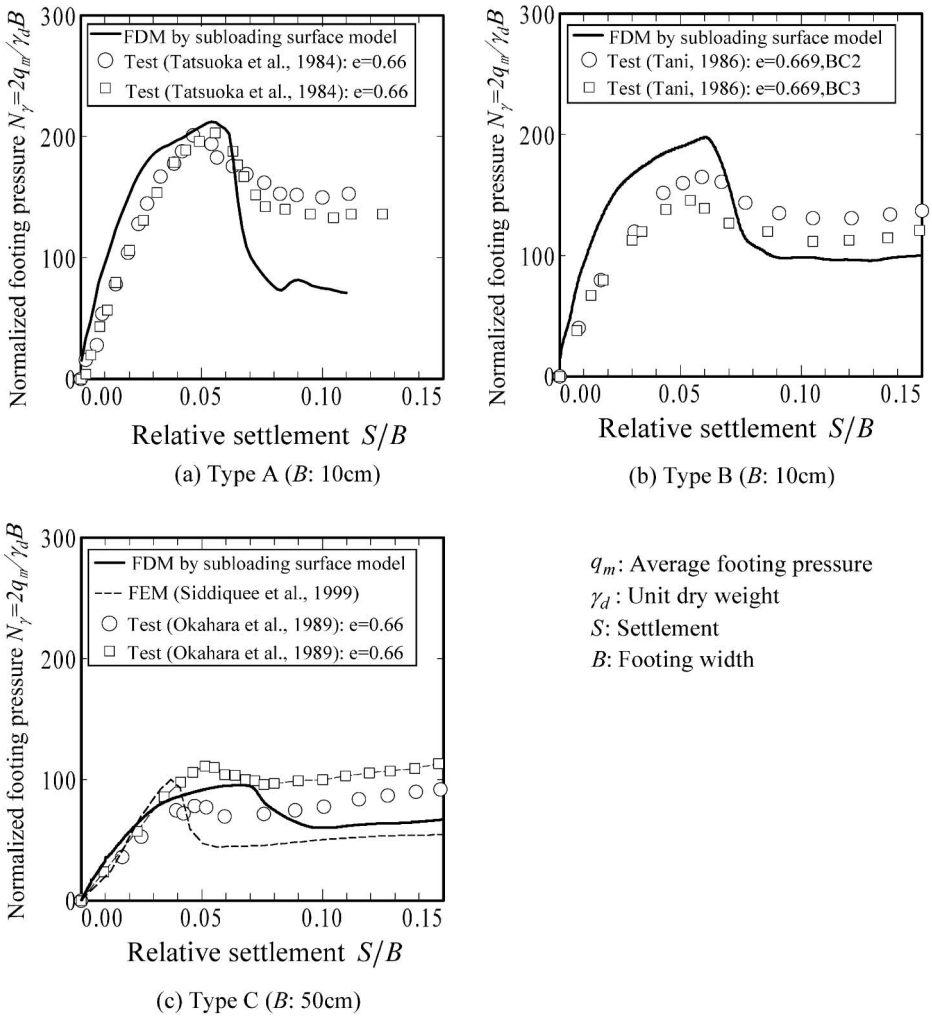

Fig. 9. Comparisons of test and calculated results for footing settlement phenomenon

stress path reducing to the null stress along and below the critical state line for loose sands and increasing along and above the critical state line for dense sands, deviating from the undrained stress path for clays exhibiting the isotropic hardening induced only by the plastic volumetric strain. The material constant p_e has only to be given a small value fulfilling $p_e > \xi F$ such that a volume does not become infinite only by the elastic deformation for the variation of pressure inside the normal-yield surface. Therein, we do not need to add a surcharge on the ground surface at null stress state. Here, note that p_e depends on F in general but this fact is ignored in the present formulation since it leads to the complexity of formulation with the elastic-plastic coupling (Hashiguchi, 2008). The values of material parameters listed above are used for all the following numerical calculations because Toyoura sands in the same initial void ratio 0.66 are used in the tests.

The comparisons of test and calculated results are shown in Fig. 9, where the prediction by Siddiquee et al. (1999) is also depicted in (c). In this figure q_m is the average footing pressure, γ_d is the unit dry weight, N_γ is the normalized footing pressure and S is the settlement. The qualitative trends of test results and the quantitative simulation to some extent are captured and the ultimate loads, i.e., bearing capacities are predicted well by the present analyses, although the analyses are performed for the sand with the high friction and dilatancy. Here, the post-peak behavior, i.e., the increase of load after exhibiting once the minimal value is also predicted well qualitatively. It would be provided by the adoption of the up-dated Lagrangian calculation leading to the accumulation of displacements of nodal points, which results in the upsurge of soils around the footing and thus the increase of footing load. However, the quantitative prediction of post-peak behavior would require further study taking account of the tangential inelastic strain rate due to the stress rate tangential to the loading surface (Hashiguchi and Tsutsumi, 2001) and the gradient effect (cf. Hashiguchi and Tsutsumi, 2006) by introducing the shear-embedded model (cf. Pietruszczak and Mroz, 1981; Tanaka and Sakai, 1993) for example.

The displacements of nodal points from the initiation of settlement are shown in Fig. 10 at the settlement 11 mm, 15 mm, 80 mm for Type A, B and C, respectively, which are the final stage of calculation. The Prantdl's slip

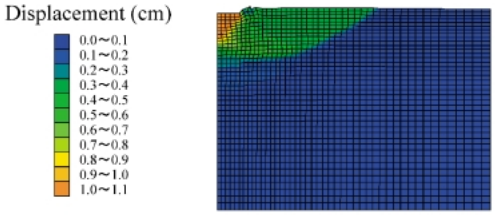

(a) Type A (B: 10cm) : Settlement=11mm

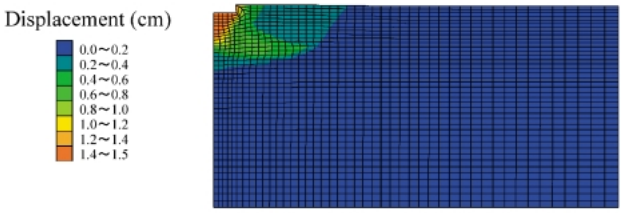

(b) Type B (B: 10cm) : Settlement=15mm

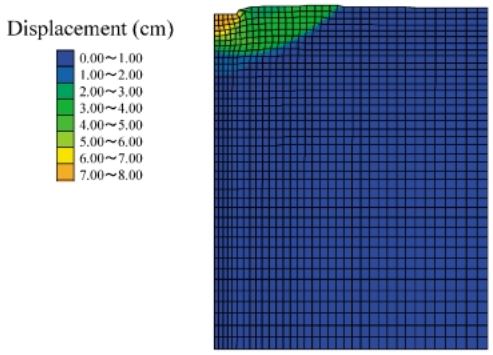

(c) Type C (B: 50cm) : Settlement=80mm

Fig. 10. Deformed finite element meshes at final step

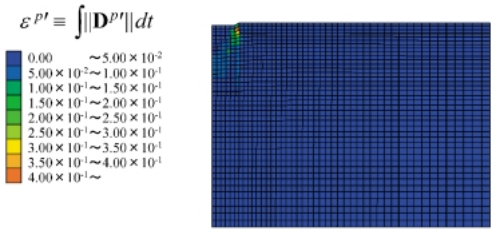

(a) Type A (B: 10cm)

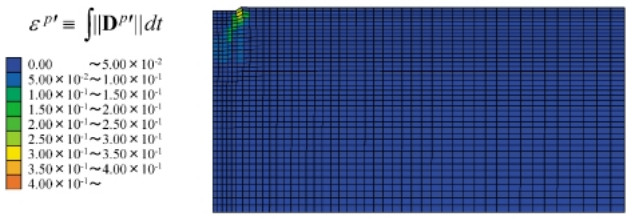

(b) Type B (B: 10cm)

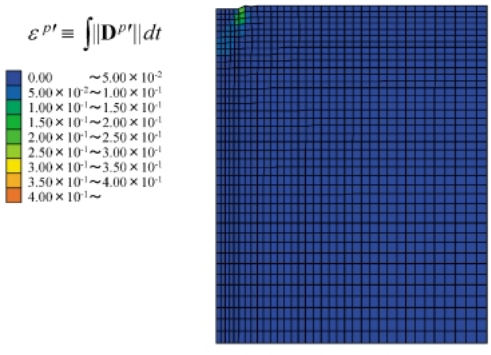

(c) Type C (B: 50cm)

Fig. 11. Distribution of accumulation of magnitude of plastic deviatoric strain rate $\varepsilon^{p\prime} \equiv \int \|\mathbf{D}^{p\prime}\| dt$ at ultimate load

line solution with the triangle wedge, the logarithmic spiral zone and the passive Rankine zone is observed clearly in this figure.

In what follows, distributions of basic physical quantities are shown based on the calculated results, which are important on the interpretation of the present problem although they are not measured or cannot be measured directly. The most basic quantities are the accumulation of magnitude of plastic deviatoric strain rate, $\varepsilon^{p\prime} \equiv \int \|\mathbf{D}^{p\prime}\| dt$ and the plastic volumetric strain ε_v^p, while they describe the loading history representatively.

The distributions of accumulation of magnitude of plastic deviatoric strain rate, $\varepsilon^{p\prime} \equiv \int \|\mathbf{D}^{p\prime}\| dt$, at the ultimate load and the final step are shown in Figs. 11 and 12, respectively. It is predicted that the slip line appears only in the vicinity of footing at the ultimate load but it develops over the wide region exhibiting the Prantdl solution at the final steps as has been revealed experimentally by Tatsuoka et al. (1992).

On the other hand, the soils in the periphery of footing inevitably experience the null or further negative pressure since they are pulled into the vertical direction as the footing settlement proceeds (*see* Fig. 13). It causes the singularity of plastic modulus for the normal-yield surface passing through the origin of stress space at which the normal-yield and the subloading surfaces contact with each other. This defect is improved in the present model by making the normal-yield surface translate to the region of negative pressure as shown in Fig. 2, whilst the numerical difficulty can be avoided although the translation was taken quite small as 1/1000 in size of the normal-yield surface. In addition, the impertinence that the volume becomes infinite elastically is avoided by shifting the isotropic consolidation characteristic into the negative range of pressures as shown in Fig. 2. It should be emphasized that the stable analysis cannot be executed without these improvements.

The distribution of plastic volumetric strain ε_v^p at final step is depicted in Fig. 14, where it is distributed widely in the upper layer of grounds. The large plastic volumetric expansion is induced in the neighborhoods of the edge of footing and along the boundary of the passive Rankine zone. Here, it is observed that the volume expansion spreads widely reaching to the side walls. The distribution of the normal-yield ratio R at the final step is shown in Fig. 15. It is known from this figure that the logarithmic spiral zone and the boundary of passive Rankine zone first reach the normal-yield state.

The differences in the distribution of mechanical quantities are observed in (a) Type A and (b) Type B of Figs.

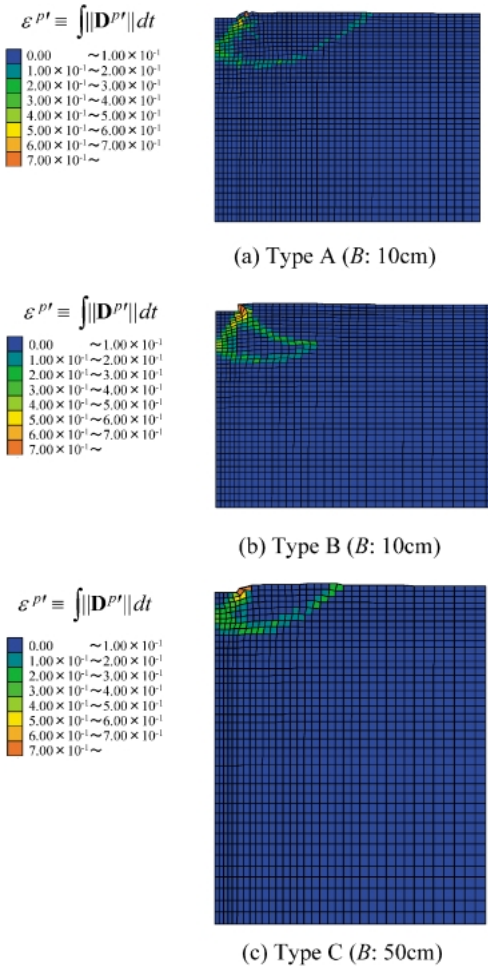

Fig. 12. Distribution of accumulation of magnitude of plastic deviatoric strain rate $\varepsilon^{p\prime} \equiv \int \|\mathbf{D}^{p\prime}\| dt$ at final step

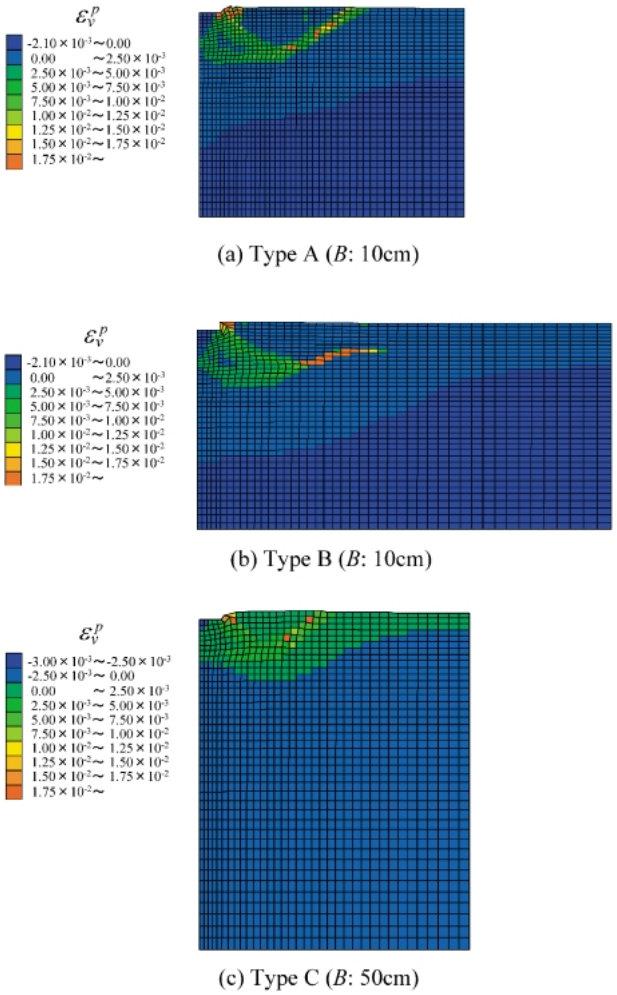

Fig. 14. Distribution of plastic volumetric strain ε_v^p at final step

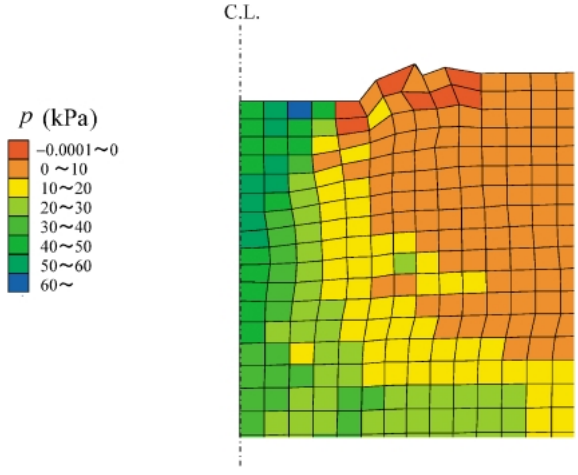

Fig. 13. Distribution of mean pressure p for type A at final step

10–15, while only the widths of soil-bins are different in these types. Then, in order to examine the influence of the width of soil-bin on the footing settlement behavior, the analyses for the three levels 80, 300 and 500 cm of soil-bin width are further performed changing the soil-bin width in the finite element mesh shown in Fig. 8(a) Type A. The distributions in the displacement of nodal points, the accumulation of magnitude of plastic deviatoric strain rate and the normal-yield ratio in the final step for the smaller soil-bin width 80 cm are shown in Fig. 16, where the clear slip-lines are observed compared with those for the soil-bin width 182 cm. Here, note that the ratio of the area of slip-line zone to the footing width is large since the active angle of internal friction is large for a small footing width as will be described later referring to Fig. 19. Then, the constraint is hard if the ratio of the soil bin width to the footing width is small. The relations of the footing load vs. the relative settlement are shown in Fig. 17, where the test data for types A and B shown in Fig. 9 are also depicted. The relation of the ultimate footing load vs. the ratio of the footing width to the soil-bin width is shown in Fig. 18. Needless to say, the footing load increases as the width of soil-bin decreases. According to the present analyses, it is required to choose the soil-bin width more than twenty times of the footing width in order to exclude the influence of the soil-bin width leading to the semi-infinite ground.

The influences of footing width on the ultimate load and the settlement at ultimate load are depicted in Fig. 19, where the calculated results by Tatsuoka et al. (1992)

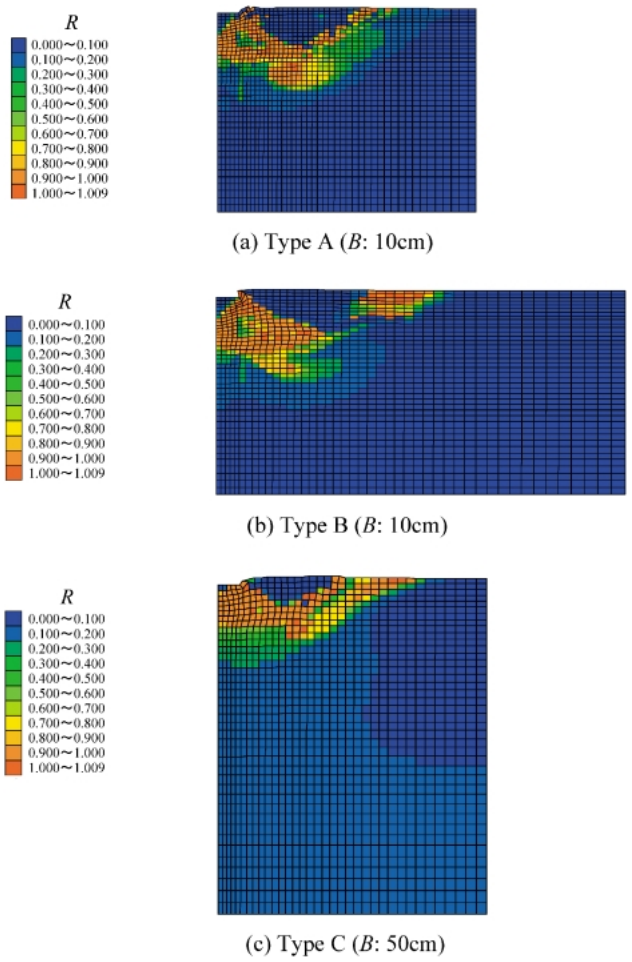

Fig. 15. Distribution of normal-yield ratio R at final step

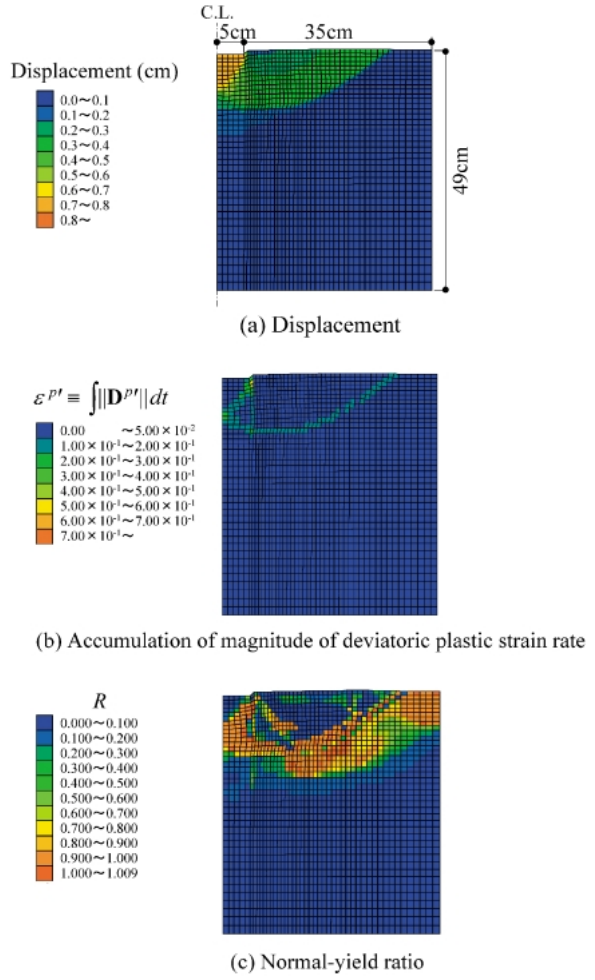

Fig. 16. Distribution of the displacement, the accumulation of magnitude of plastic deviatoric strain rate $\varepsilon^{p\prime} \equiv \int \|\mathbf{D}^{p\prime}\| dt$ and the normal-yield ratio R at final step (Settlement = 8 mm) (B: 10 cm, L: 80 cm)

are also depicted. The finite element meshes scaled up or down from the mesh in Fig. 8 for type B (footing width 10 cm) in proportion to the footing width are adopted in these analyses. The test results that the ultimate footing pressure increases quite intensely as the footing width decreases are predicted fairly well by the calculations on the contrary to the simple interpretation that the compressive stress in soils increases by the weight of soils themselves and thus the ultimate footing pressure increases as the footing width increases. It was interpreted by Siddiquee et al. (1999) for this fact that the active angle of internal friction increases as the pressure decreases. This property is reflected in the present model predicting the decrease of stress ratio at failure with the increase of the pressure, while it is lacking in the Drucker-Prager model (1952) without the cohesion. The dependence of failure stress on the pressure is shown in Fig. 20, while the settlement at ultimate load is hardly affected by the footing width in both the test and calculated results.

The pertinent result for the footing-settlement problem on the sand with a high friction, one of the difficult problems in soil mechanics, is obtained in the present study as described above. Here, the peak, the subsequent reduction and the final increase of footing load are predicted well qualitatively and quantitatively to some extent.

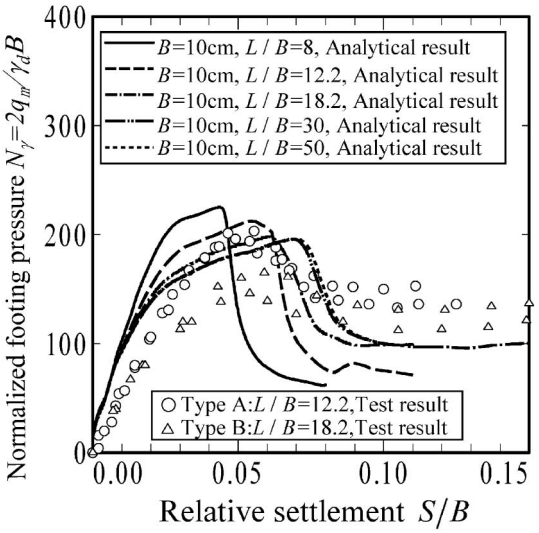

Fig. 17. Influence of ratio of soil-bin and footing width on footing load-settlement relation

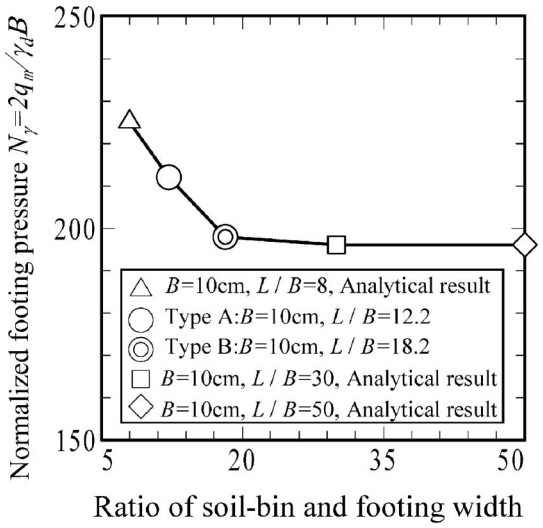

Fig. 18. Predicted influence of ratio of soil-bin width to footing width on ultimate load

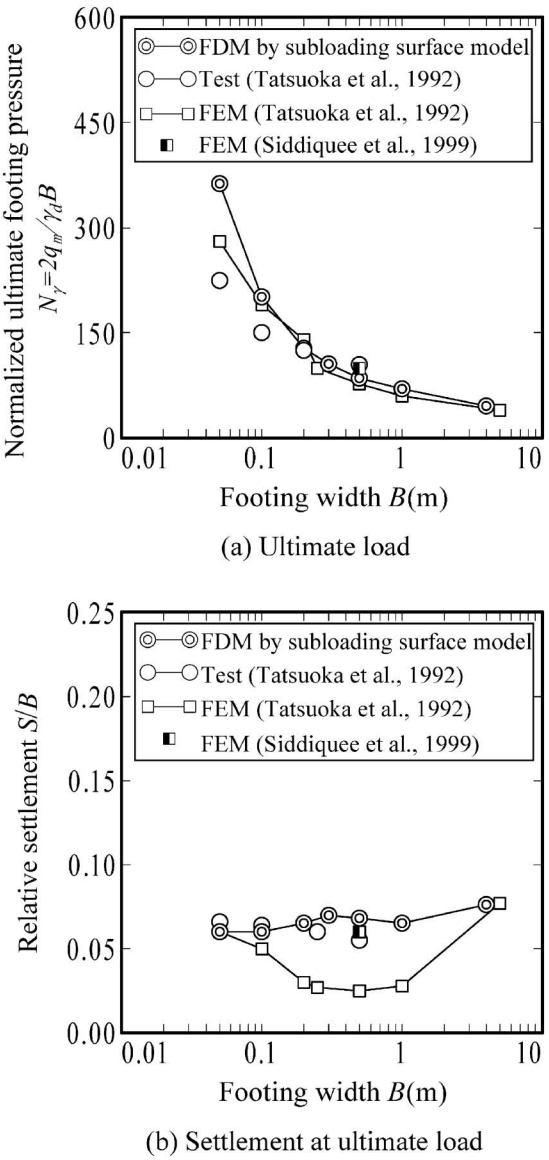

Fig. 19. Influences of footing width

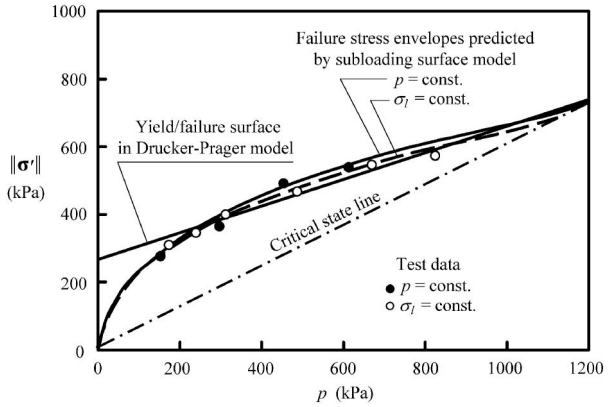

Fig. 20. Dependence of failure stress on pressure (Hashiguchi et al., 2002)

The reasons for successful outcome are summarized as follows:

1) The subloading surface model applied in the present analysis has the following advantages:
   i) It is furnished with the automatic controlling function to attract the stress to the yield surface, whilst all other elastoplastic constitutive models are required to incorporate a return-mapping algorithm to pull back the stress to the yield surface in the plastic deformation process in the normal-yield state as shown in Fig. 4. The distinguished advantage enables us to execute an accurate calculation by the program FLAC3D adopting the simple Euler method without a convergence calculation process.
   ii) It is not required of the judgment whether or not the yield condition is fulfilled in the loading criterion.
   iii) It adopts the associativity of the flow rule and thus leads to the symmetry of elastoplasic constitutive matrix. Therefore, this model possesses the distinguishable adaptability to numerical calculation.
2) The subloading surface model of soils applied in the present analysis has the advantages:
   i) It is capable of describing the softening behavior and dilatancy characteristics quite realistically, predicting the simultaneous occurrence of the peak load and the highest dilatancy rate as has been found experimentally by Taylor (1948).
   ii) It has the full regularity since the normal-yield surface does not pass through the zero stress point and thus the subloading surface is always determined uniquely. In addition, the elastic property is improved such that the elastic bulk modulus does not become zero for the stress inside the normal-yield surface.
3) The finite difference program FLAC3D adopted in the present study is based on the explicit-relaxation method which enables us to shorten the calculation time drastically since it is not required to solve the total stiffness matrix.

CONCLUDING REMARKS

The footing-settlement problem on the sand with a

high friction and dilatancy is analyzed in this study. The numerical analysis incorporating the subloading surface model into the finite difference program based on the dynamic-relaxation method is performed and it revealed that a pertinent prediction is attained exhibiting high efficiency and robustness. The numerical analysis due to the subloading surface model presented in this study has the distinguishable efficiency and the robustness. Now, it could be stated that the present numerical method can take the place of the slip-line method which has been used for the practical design of soil structures for a long time and the para-elastoplastic model (e.g., Duncan and Chang, 1970).

However, the pertinent prediction of deformation in the post-peak stress state requires the incorporation of the tangential inelastic strain rate (Hashiguchi and Tsutsumi, 2001, 2003; Hashiguchi and Protasov, 2004; Khojastehpour and Hashiguchi, 2004a, b; Tsutsumi and Hashiguchi, 2005) and the further study considering the shear band leading to avoid the mesh size dependency which would be the quite difficult issue. One of approaches to consider the shear band is the incorporation of the smeared (shear-band embedded) model (Pietrueszczak and Mroz, 1981; Tanaka and Kawamoto, 1988; Tanaka and Sakai, 1993), while the gradient-dependent models (Aifantis, 1984; Vardoulakis and Sulem, 1995; Hashiguchi and Tsutsumi, 2006), the non-local theories (Bazant and Cedolin, 1991) and the Cosserat models (Muhlhaus and Vardoulakis, 1987) would be rigorous theoretically but are inapplicable to numerical analyses in engineering practice since one cannot use finite elements far smaller than shear-band width because of the limitation of computer capacity at least at present. In addition, the anisotropy due to the rotational hardening (Hashiguchi and Chen, 1998; Hashiguchi, 2001) is required since soil grounds *in situ* exhibit the anisotropy induced during the K_o-consolidation process. Further study considering these fundamental issues has to be performed progressively.

ACKNOWLEDGEMENTS

The authors would like to express sincere gratitude to Prof. Tadatsugu TANAKA, University of Tokyo and Prof. Yuki YAMAKAWA, Tohoku University for the valuable discussions and advices to numerical analyses in this study.

REFERENCES

1) Aifantis, E. C. (1984): On the microstructure origin of certain inelastic models, *J. Eng. Mat. Tech.*, ASME, **106**, 326–334.
2) Alonso, E. E., Gens, A. and Josa, A. (1990): A constitutive model for partially saturated soils, *Geotechnique*, **40**, 405–430.
3) Bazant, Z. P. and Cedolin, L. (1991): *Stability of Structures*, Oxford Univ. Press.
4) Borja, R. I. and Lee, S. R. (1990): Cam-clay plasticity, Part I: Implicit integration of elasto-plastic constitutive relations, *Comp. Meth. Appl. Mech. Eng.*, **78**, 49–72.
5) Borja, R. I. (1991): Cam-clay plasticity, Part II: Implicit integration of constitutive equation based on a nonlinear elastic stress predictor, *Comp. Meth. Appl. Mech. Eng.*, **88**, 225–240.
6) Borja, R. I. and Tamagnini, C. (1998): Cam-clay plasticity, Part III: Extension of the infinitesimal model to include finite strains, *Comp. Meth. Appl. Mech. Eng.*, **155**, 73–95.
7) Borja, R. I., Lin, C.-H. and Montans, F. J. (2001): Cam-clay plasticity, Part IV: Implicit integration of anisotropic bounding surface model with nonlinear hyperelastic and ellipsoidal loading function, *Comp. Meth. Appl. Mech. Eng.*, **190**, 3293–3323.
8) Borja, R. I., Sama, K. M. and Sanz, P. F. (2003): On the numerical integration of three-invariant elastoplastic constitutive models, *Comp. Meth. Appl. Mech. Eng.*, **192**, 1227–1258.
9) Borja, I. (2004): Cam-clay plasticity, Part V: A mathematical framework for three-phase deformation and strain localization analyses of partially saturated porous media, *Comp. Meth. Appl. Mech. Eng.*, **193**, 5301–5338.
10) Cundall, P. and Board, M. (1988): A microcomputer program for modeling large-strain plasticity problems, *Prepare for the 6th Int. Conf. Numer. Meth. Geomech.*, Innsbruck, Austria, 2101–2108.
11) Dafalias, Y. F. and Herrmann, L. R. (1982): Bounding surface formulation of soil plasticity, *Soil Mech.-Trans. Cyclic Load* (eds. by Pande, G. N. and Zienkiewicz, O. C.), John Wiley & Sons, Chichester, 253–282.
12) de Borst, R., Sluys, L. J., Muhlhaus, H. B. and Pamin, J. (1993): Fundamental issues in finite element analyses of localization of deformation, *Eng. Comput.*, **10**, 99–121.
13) de Borst, R. and Groen, A. E. (1999): Towards efficient and robust elements for 3-D plasticity, *Comput. Struct.*, **70**, 23–34.
14) Drucker, D. C. and Prager, W. (1952): Soil mechanics and plastic analysis or limit design, *Quart. Appl. Math.*, **10**, 157–165.
15) Drucker, D. C. (1988): Conventional and unconventional plastic response and representation, *Appl. Mech. Rev.*, ASME, **41**, 151–167.
16) Duncan, J. M. and Chang, C. Y. (1970): Nonlinear analysis of stress and strain in soils, *J. Soil Mech. Fund. Div.*, ASCE, **96**, 1629–1653.
17) Hashiguchi, K. (1974): Isotropic hardening theory of granular media, *Proc. Japan Soc. Civil Eng.*, (227), 45–60.
18) Hashiguchi, K. and Ueno, M. (1977): Elastoplastic constitutive laws of granular materials, *Constitutive Equations of Soils* (*Proc. 9th ICSMFE, Spec. Session 9*, Tokyo), JSSMFE, 73–82.
19) Hashiguchi, K. (1978): Plastic constitutive equations of granular materials, *Proc. US-Japan Seminar Continuum Mech. Statistical Approach for Granular Materials*, Sendai, 321–32.
20) Hashiguchi, K. (1980): Constitutive equations of elastoplastic materials with elastic-plastic transition, *J. Appl. Mech.*, ASME, **47**, 266–272.
21) Hashiguchi, K. (1989): Subloading surface model in unconventional plasticity, *Int. J. Solids Struct.*, **25**, 917–945.
22) Hashiguchi, K. (1993a): Fundamental requirements and formulation of elastoplastic constitutive equations with tangential plasticity, *Int. J. Plasticity*, **9**, 525–549.
23) Hashiguchi, K. (1993b): Mechanical requirements and structures of cyclic plasticity models, *Int. J. Plasticity*, **9**, 721–748.
24) Hashiguchi, K. (1995): On the linear relations of V-ln p and ln v-ln p for isotropic consolidation of soils, *Int. J. Numer. Anal. Meth. Geomech.*, **19**, 367–376.
25) Hashiguchi, K. (1997): The extended flow rule in plasticity, *Int. J. Plasticity*, **13**, 37–58.
26) Hashiguchi, K. and Chen, Z.-P. (1998): Elastoplastic constitutive equation of soils with the subloading surface and the rotational hardening, *Int. J. Numer. Anal. Meth. Genomic.*, **22**, 197–227.
27) Hashiguchi, K. (2000): Fundamentals in constitutive equation: Continuity and smoothness conditions and loading criterion, *Soils and Foundations*, **40**(3), 155–161.
28) Hashiguchi, K. (2001): Description of inherent/induced anisotropy of soils: Rotational hardening rule with objectivity, *Soils and Foundations*, **41**(6), 139–145.
29) Hashiguchi, K. and Tsutsumi, S. (2001): Elastoplastic constitutive equation with tangential stress rate effect, *Int. J. Plasticity*, **17**,

117–145.
30) Hashiguchi, K. (2002): A proposal of the simplest convex-conical surface for soils, *Soils and Foundations*, **42**(3), 107–113.
31) Hashiguchi, K., Saitoh, K., Okayasu, T. and Tsutsumi, S. (2002): Evaluation of typical conventional and unconventional plasticity models for prediction of softening behavior of soils, *Geotechnique*, **52**, 561–578.
32) Hashiguchi, K. and Tsutsumi, S. (2003): Shear band formation analysis in soils by the subloading surface model with tangential stress rate effect, *Int. J. Plasticity*, **19**, 1651–1677.
33) Hashiguchi, K. and Protasov, A. (2004): Localized necking analysis by the subloading surface model with tangential-strain rate and anisotropy, *Int. J. Plasticity*, **20**, 1909–1930.
34) Hashiguchi, K. and Tsutsumi, S. (2006): Gradient plasticity with the tangential subloading surface model and the prediction of shear band thickness of granular materials, *Int. J. Plasticity*, **22**, 767–797.
35) Hashiguchi, K. (2007): General corotational rate tensor and replacement of material-time derivative to corotational derivative of yield function, *Comput. Model. Eng. Sci.*, **17**, 55–62.
36) Hashiguchi, K. and Mase, T. (2007): Extended yield condition of soils with tensile yield strength and rotational hardening, *Int. J. Plasticity*, **23**, 1939–1956.
37) Hashiguchi, K. (2008): Verification of compatibility of isotropic consolidation characteristics of soils to multiplicative decomposition of deformation gradient, *Soils and Foundations*, **48**(4), 597–602.
38) Hill, R. (1967): On the classical constitutive relations for elastic/plastic solids, *Recent Progress in Appl. Mech. (The Folke Odqvist Volume)*, John-Wiley and Sons, Chichester, 241–249.
39) Itasca Consulting Group (2006): *FLAC3D, Fast Lagrangian Analysis of Continua in 3 Dimensions*, Minneapolis, Minnesota, USA.
40) Iwan, W. D. (1967): On a class of models for the yielding behavior of continuous and composite systems, *J. Appl. Mech.*, ASME, **34**, 612–617.
41) Jaumann, G. (1911): Geschlossenes system physicalisher und chemischer differentialgesetze, *Sitzber. Akad. Wiss. Wien* (IIa), **120**, 385–530.
42) Khojastehpour, M. and Hashiguchi, K. (2004a): Axisymmetric bifurcation analysis of soils by the tangential-subloading surface model, *Int. J. Solids Struct.*, **41**, 5541–5563.
43) Khojastehpour, M. and Hashiguchi, K. (2004b): The plane strain bifurcation analysis of soils by the tangential-subloading surface model, *J. Mech. Physics of Solids*, **52**, 2235–2262.
44) Lee, E. H. (1969): Elastic-plastic deformation at finite strains, *J. Appl. Mech.*, ASME, **36**, 1–6.
45) Muhlhaus, H. B. and Vardoulakis, I. (1987): The thickness of shear bands in granular materials, *Geotechnique*, **37**, 271–283.
46) Nakano, M., Yamada, E. and Noda, T. (2008): Ground improvement of intermediate reclaimed land by compaction through cavity expansion of sand piles, *Soils and Foundations*, **48**(5), 653–672.
47) Noda, T., Asaoka, A. and Yamada, S. (2007): Some bearing capacity characteristics of a structured naturally deposited clay soil, *Soils and Foundations*, **47**(2), 285–301.
48) Okahara, M., Takagi, S., Mori, H., Koike, S., Tatsuda, M., Tatsuoka, F. and Morimoto, H. (1989): Large scale plane strain bearing capacity tests of shallow foundation on sand (Part 1), *Proc. 24th Annual Meeting Japan. Soc. Geotech. Eng.*, 1239–1242.
49) Pietruszczak, S. T. and Mroz, Z. (1981): Finite element analysis of deformation of strain softening materials, *Int. J. Numer. Meth. Eng.*, **17**, 327–334.
50) Pietruszczak, S. T. and Niu, X. (1993): On the description of localized deformation, *Int. J. Numer. Anal. Meth. Geomech.*, **17**, 791–805.
51) Potts, D. M. (2003): Numerical analysis: a virtual dream or practical reality?, *Geotechnique*, **53**, 535–573.
52) Roscoe, K. H. and Burland, J. B. (1968): On the generalized stress-strain behavior of 'wet' clay, *Engineering Plasticity* (eds. by Heyman, J. and Leckie, F. A.), Cambridge Univ. Press, 535–608.
53) Schofield, A. N. and Wroth, C. P. (1968): *Critical State Soil Mechanics*, McGraw-Hill, London.
54) Setouchi, H. and Hashiguchi, K. (2006): Research on determination of material parameters of the subloading surface model, *Journal of Applied Mechanics (JSCE)*, **9**, 491–502 (in Japanese).
55) Sheng, D., Sloan, S. W. and Yu, H. S. (2000): Aspects of finite element implementation of critical state models, *Computational Mechanics*, **26**, 185–196.
56) Siddiquee, M. S. A., Tanaka, T., Tatsuoka, F., Tani, K. and Morimoto, T. (1999): Numerical simulation of bearing capacity characteristics of strip footing on sand, *Soils and Foundations*, **39**(4), 93–109.
57) Siddiquee, M. S. A., Tatsuoka, F., Tanaka, T., Yoshida, K., Tani, K. and Morimoto, T. (2001): Model tests and FEM simulation of some factors affecting the bearing capacity of a footing on sand, *Soils and Foundations*, **41**(2), 53–76.
58) Simo, J. C. and Meschke, G. (1993): A new algorithms for classical plasticity extended to finite strains, application to geomaterials, *Comput. Mech.*, **11**, 253–287.
59) Simo, J. C. and Hughes, T. J. R. (1998): *Computational Plasticity*, Springer.
60) Sloan, S. W. and Randolph, M. F. (1982): Numerical prediction of collapse loads using finite element methods, *Int. J. Numer. Anal. Meth. Geomech.*, **6**, 47–76.
61) Smith, I. M. and Griffith, V. (2004): *Programming the Finite Element Method*, 4th Edition, John-Wiley.
62) Stallebrass, S. E. and Taylor, R. N. (1997): The development and evaluation of a constitutive model for the prediction of ground movements in overconsolidated clay, *Geotechnique*, **47**, 235–253.
63) Tanaka, T. and Kawamoto, O. (1988): Three dimensional finite element collapse analysis for foundations and slopes using dynamic relaxation, *Proc. Numer. Meth. Geimech.*, Insbruck, 1213–1218.
64) Tanaka, T. and Sakai, T. (1993): Progressive failure and scale effect of trap-door problems with granular materials, *Soils and Foundations*, **33**(1), 11–22.
65) Tani, K. (1986): Mechanism of bearing capacity of shallow foundation, *Master Thesis*, Univ. Tokyo.
66) Tatsuoka, F., Ikuhara, O, Fukushima, S. and Kawamura, T. (1984): On the relation of bearing capacity of shallow footing on model sand ground and element test strength, *Proc. Symp. Asses. Deform. & Fail. Strength of Sandy Soils and Sand Grounds*, Japan. Soc. Geotech. Eng., 141–148.
67) Tatsuoka, F., Okahara, M., Tanaka, T. and Siddiquee, M. S. A. (1992): Study into the bearing capacity of strip footing on sand by model tests, element tests and numerical analyses, *Tsuchi-to-Kiso (J. Japan. Soc. Geotech. Eng.)*, **40–5**, 11–16.
68) Taylor, D. W. (1948): *Fundamentals of Soil Mechanics*, John Wiley & Sons.
69) Tsutsumi, S. and Hashiguchi, K. (2005): General non-proportional loading behavior of soils, *Int. J. Plasticity*, **21**, 1941–1969.
70) Vardoulakis, I. and Sulem. J. (1995): *Bifurcation Analysis in Geomechanics*, Blackie Academic & Professional, London.
71) Yamakawa, Y., Ikeda, K. and Tsutsumi, S. (2003): Simulation and interpretation of diffuse mode bifurcation of elastoplastic solids, *J. Mech. Phys. Solids*, **51**, 1649–1673.